Semiempirical hypotheses of turbulence theory in the anisotropic boundary layer

V.V. Nosov, O.N. Emaleev, V.P. Lukin, and E.V. Nosov

Institute of Atmospheric Optics,
Siberian Branch of the Russian Academy of Sciences, Tomsk

Received February 22, 2005

It has been stated that the theory of similarity of turbulent flows can be propagated to an arbitrary anisotropic boundary layer. With the use of semiempirical hypotheses of the turbulence theory, it is theoretically and experimentally shown that an arbitrary anisotropic boundary layer can be considered the locally weakly anisotropic. Except for the tensor of the turbulent thermal diffusivity coefficients, the theoretical propositions of an isotropic layer (for plane-parallel flows) are carried out in the vicinity of every point of the layer. In an arbitrary boundary layer, the key turbulence parameter is the varying Monin–Obukhov number. It is established that the anisotropic boundary layer can be substituted for an effective isotropic layer. Theoretical expressions are obtained for the vertical outer scale of turbulence in the anisotropic boundary layer; the coincidence of the experimental and theoretical values of the outer scale of turbulence is shown.

Introduction

As is generally known, the turbulence theory originates from the description of liquid and gas flows on the basis of the hydrodynamic equations. A full statistical description of the accidental hydrodynamic fields can be presented by the characteristic functional.[1,3,4] The characteristic functional contains information about the infinite set of moments of fields and fits dynamic equations with functional derivatives. At present, acceptable methods for solution of such equations are not available. At the same time, for many practical applications it is sufficient to determine only the statistical moments of the lowest orders. Therefore, by tradition, the researches in the turbulence theory are based on a set of the Reynolds equations, resulting from averaging of the hydrodynamic equations.[1–6] However, in the set of the Reynolds equations, the number of unknowns exceeds the number of equations. A closure of this system is usually performed via setting some relations between moments of hydrodynamic fields. The relations found experimentally or obtained from the physical reasons (for example, from the dimensionality reasons), are termed semiempirical hypotheses of the turbulence theory.

The basic semiempirical hypotheses are usually reduced to setting relations between the second moments of the velocity $\overline{v'_i v'_j}$ and temperature $\overline{v'_j T'}$ pulsations (deviations from average) and the averaged velocity and temperature fields $\overline{T}$. These hypotheses are based, as a rule, on analogy between the turbulent and molecular motions. Thus, the terms $\nu\partial\overline{v_i}/\partial x_j$ and $\chi\partial\overline{T}/\partial x_j$ presented in the averaged equations are proportional to the flow components of the momentum and heat (ν is the kinematic viscosity; χ is the thermal diffusivity). They are caused by the molecular diffusion and describe the medium free of turbulence. In the turbulent medium, $-\overline{v'_i v'_j}$ and $-\overline{v'_j T'}$ are added to the indicated components, respectively. Therefore, these quantities can be considered as components of turbulent flows of the momentum and heat. In terms of the semiempirical theory, the structure of dependence of turbulent flows of the momentum and heat on $\overline{v_i}$ and $\overline{T}$ is the same, as in case of purely molecular diffusion. In general case of the anisotropic turbulence[1]

$$\overline{v'_i v'_j} = \overline{v'_n v'_n}\delta_{ij}/3 - (K_{in}\Phi_{nj} + K_{jn}\Phi_{ni})/2;$$
$$\Phi_{ij} = \partial\overline{v_i}/\partial x_j + \partial\overline{v_j}/\partial x_i;$$
$$\overline{v'_j T'} = -K_{Tji}\partial\overline{T}/\partial x_i, \qquad (1)$$

where the repeating indices stand for summation. The components K_{ij} of the symmetric tensor K in definitions (1) are the turbulent viscosity coefficients, and the components K_{Tij} of the tensor K_T are the turbulent thermal diffusivity coefficients or the turbulent diffusion coefficients for a passive impurity, which is the potential temperature T (in a boundary layer, the standard and potential temperatures can be the same). Hypotheses (1) replace 12 components of turbulent flows of the momentum and heat for 27 new quantities (by 6 components in symmetric tensors K_{ij} and Φ_{ij}, nine in tensor K_{Tij}, three derivatives $\partial\overline{T}/\partial x_i$ and three components in the sum $\overline{v'_n v'_n}$).

It is generally known[1,3–7] that in plane-parallel flows (between separated planes and in tubes) the turbulent phenomena in a boundary layer are well described by semiempirical hypotheses with application of only two scalar parameters K and K_T

0235-6880/05/10 756-17 $02.00

(the turbulent viscosity coefficient and the turbulent thermal diffusivity, respectively). The turbulence in an atmospheric boundary layer can be considered a particular case of the plane-parallel flow when considering flows above extended ground areas with a smooth, homogeneous (identical by structure), and equally heated surface. As equations (1) show, the K and K_T tensors are isotropic ($K_{ij} = K\delta_{ij}$, $K_{Tij} = K_T\delta_{ij}$) for plane-parallel flows. In this connection, a boundary layer with the isotropic tensors K and K_T will be called for brevity the isotropic boundary layer. If at least one of K and K_T is anisotropic, the boundary layer is called anisotropic.

In practice, however, these definitions must be more comprehensive. Thus, the isotropic boundary layer turns out to be a more general notion, than the boundary layer in plane-parallel flows. Unlike the plane-parallel flows, in an isotropic layer in a general case the conditions can be realized, under which the horizontal derivatives and a vertical component of mean velocity are not zero. It is naturally to call such a layer weakly isotropic, attributing the notion of isotropic (or strongly isotropic) boundary layer only to plane-parallel flows. The similar division can be conducted also for the anisotropic boundary layer. Thus, if one of the tensors K or K_T is anisotropic, then the boundary layer can be called weakly anisotropic. If the both tensors are anisotropic, then the layer is called strongly anisotropic.

The notion of the isotropic boundary layer (for plane-parallel flows) is not connected with the isotropy of the hydrodynamic fields themselves. There is a preferential direction (the distance from the boundary plane) in the isotropic layer, therefore, the fields will not be isotropic.

Components of tensors K and K_T can be presented as products of the root-mean-square values of velocity pulsations on the tensor components of the turbulence scales l_{ij}, l_{Tij} (scales are the mean distances, to which turbulent formations are capable to move keeping their individuality)

$$K_{ij} = \overline{v'_n v'_n}^{1/2} l_{ij},\ K_{Tij} = \overline{v'_n v'_n}^{1/2} l_{Tij}.$$

For isotropic tensors K and K_T, the scale ellipsoids l_{ij} and l_{Tij} are transformed into a sphere. Generally, tensors l_{ij} and l_{Tij} do not coincide. The variability of temperature scales l_{Tij} is commonly higher, than of velocity scales l_{ij}. This is evident in case of free convection, when wind and friction are absent. Then turbulence receives the energy not from the averaged motion energy, but from the temperature instability energy and has a character of vertical thermal flows. Therefore, in the first approximation, tensor K in Eq. (1) can be considered isotropic ($\overline{v'_i v'_j}$ remains anisotropic in any case). Then[1,6]

$$\overline{v'_i v'_j} = \overline{v'_n v'_n}\,\delta_{ij}/3 - K(\partial\overline{v}_i/\partial x_j + \partial\overline{v}_j/\partial x_i),$$
$$\overline{v'_j T'} = -K_{Tji}\,\partial\overline{T}/\partial x_i \qquad (2)$$

and the number of unknowns decreases to 22.

Semiempirical hypotheses are actively used in studies of the turbulent diffusion of passive impurities, including the temperature diffusion. The hypotheses (2) are usually taken as fundamental. Expressions accepted at present for K, K_{Tij} resulted from generalization of the experimental data obtained above approximately even surface (not in mountain regions), and take into account the effect of thermal stratification. For mean wind velocity[1] directed along the axis x_1

$$K_{Tij} = \beta_{ij} K_T,\ K_T/K = \alpha,\ \alpha = Pr^{-1}, \qquad (3)$$
$$\beta_{33} = 1,\ \beta_{11} = 8.04,\ \beta_{22} = 4.21,\ \beta_{13} = -3.51,$$
$$\beta_{31} = -0.49,\ \beta_{12} = \beta_{21} = \beta_{23} = \beta_{32} = 0,$$
$$K = K(z) = æV_* z/\varphi(\zeta),\ \zeta = z/L,$$
$$K_T = K_T(z) = \alpha(z)\,K(z)$$

(the error in determination of β_{ij} does not exceed[1] 30%). Here æ = 0.4 is the Karman constant; z is the height above the underlying surface ($x_1 = x$, $x_2 = y$, $x_3 = z$); $\varphi(\zeta)$ is the universal similarity function specifying the stratification type (Fig. 1).

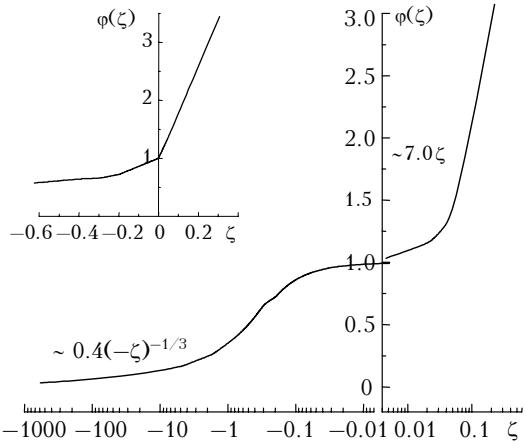

Fig. 1. Universal similarity function $\varphi(\zeta)$, constructed via joining empirical values (the plot at the top left, the data by A.S. Gurvich (Ref. 7)) with the known asymptotics[1]: $\varphi(\zeta) = 0.4(-\zeta)^{-1/3}$, $\zeta < 0$, $|\zeta| << \zeta_0$; $\varphi(\zeta) = 7.0\zeta$, $\zeta >> \zeta_0$; $\zeta_0 = 0.05$ (the error in measurement of 0.4 coefficient is about 20%, 7.0 coefficient – about 40%).

The similarity function depends on the stratification parameter $\zeta = z/L$, in which the scaling length L is termed the Monin–Obukhov scale (or the sublayer thickness of the dynamic turbulence). The length L has a fundamental significance in theory of thermally stratified atmosphere. It was coined by A.S. Monin and A.M. Obukhov (Ref. 2) from dimensionality reasons as

$$L = V_*^2/(\alpha æ^2 \beta T_*),\ \beta = g/\overline{T};$$
$$V_*^2 = -\overline{v'_1 v'_3};\ \alpha æ V_* T_* = -\overline{v'_3 T'}, \qquad (4)$$

where g is the acceleration of gravity; $\overline{T}$ is the mean value of absolute temperature; V_* is the friction velocity (the turbulent velocity scale); T_* is the

turbulent scale of the temperature field. For indifferent stratification parameter ζ coincides with the dynamic Richardson number Rf ($Rf = \zeta/\varphi(\zeta)$, $Ri = Rf/\alpha$). Therefore, by analogy with the Richardson number, ζ is often termed the Monin–Obukhov number. Experimental data for the $\alpha(\zeta) = K_T/K$ show that at indifferent ($|\zeta| \le 0.05$) and unstable ($\zeta < -0.05$) stratification the $\alpha(\zeta)$ is close to constant, $\alpha \approx 1.17$, $Pr \approx 0.85$ (Pr is the turbulent Prandtle number).[1] However, at a stable stratification ($\zeta > +0.05$) it can appreciably decrease (at a strong stability).

In expressions (3) and (4) the turbulent viscosity coefficient $K(z)$ corresponds to the isotropic boundary layer, in which V_*, T_*, and $\overline{T}$ are considered constant throughout the layer. Therefore, the Monin–Obukhov scale L and the Monin–Obukhov number ζ (at a set height z) are numerical parameters of the turbulent flow above the entire temperature-stratified region of the ground surface under observation. As relations (3) show, the K_T tensor is anisotropic, i.e., the boundary layer (2)–(4) is also anisotropic. Since the anisotropy of a boundary layer of the turbulent diffusion (2)–(4) is caused only by the K_{Tij} temperature tensor anisotropy, and other characteristics correspond to isotropic layer, the boundary layer (2)–(4) is weakly anisotropic.

Relations (2)–(4) are fundamental in the similarity theory of turbulent atmospheric flows, commonly called the Monin–Obukhov similarity theory.

The turbulent motions in mountain regions are of a special interest. Here, the constancy of the Monin–Obukhov scale is not expected above the entire territory. There are stable vortex formations above the mountain relief. The air flow disturbances from such rotary formations are observed up to high altitudes (from a mountain height, for example, of 1 km up to 7–9 km (Ref. 8)). At the same time, in atmospheric-optics researches, in particular, in researches of the turbulence influence on the optical image quality, it is often necessary to deal with the anisotropic boundary layer in mountains (the surface receiving telescopes are usually located at mountain peaks in order to decrease the turbulent distortions). However, the turbulence models developed for the isotropic boundary layer, are not applicable in mountains. Estimation of the anisotropic layer model (2)–(4) applicability to mountains has not been carried out. Therefore, the experimental testing of semiempirical hypotheses (1) or (2) directly for mountain conditions is of interest. Earlier, such testing was not carried out in a necessary volume, because it was connected with the necessity of simultaneous recording of experimental data for a large number of parameters in each point of a chosen mountain region.

In this work, it is theoretically and experimentally shown with the use of semiempirical hypotheses of the turbulence theory that an arbitrary anisotropic boundary layer can be considered a locally weakly anisotropic. Except for the tensor of the turbulent thermal diffusivity coefficients, the principles of the isotropic layer theory (for plane-parallel flows) are true in the vicinity of every point of the layer. In an arbitrary boundary layer, the key turbulence parameter is the varying Monin–Obukhov number. It is established, that the anisotropic boundary layer can be substituted for an effective isotropic layer. Theoretical expressions are obtained for the vertical outer scale of turbulence in the anisotropic boundary layer; the coincidence of the experimental and theoretical values of the outer scale is shown.

1. Theoretical representations for dissipation rates of the kinetic energy ε and temperature N in the anisotropic boundary layer

The average values of dissipation rates for the kinetic energy ε and temperature fluctuations N are important physical characteristics of the turbulent motion in a medium. They determine the intensity of velocity and temperature fluctuations. According to the Kolmogorov–Obukhov law, the structural functions of the longitudinal velocity $D_{rr}(r)$ and temperature $D_T(r)$ fluctuations in the inertial interval of r scales are expressed through ε and N:

$$D_{rr}(r) = C_V^2 r^{2/3} \; (C_V^2 = C\varepsilon^{2/3}),$$
$$D_T(r) = C_T^2 r^{2/3} \; (C_T^2 = C_\theta \varepsilon^{-1/3} N), \qquad (5)$$

where C and C_θ are the Kolmogorov and Obukhov constants, respectively, their numerical values with 10% error are equal[1] to 1.9 and 3.0, respectively. Parameters C_V^2 [$(m/s)^2 \cdot cm^{-2/3}$] and C_T^2 [$deg^2 \cdot cm^{-2/3}$] are structural characteristics of fluctuations of the longitudinal velocity and temperature. Values of ε and N are expressed[1,3] through the statistical moments $\overline{v_i' v_j'}$, $\overline{v_j' T'}$:

$$\varepsilon = -\overline{v_i' v_j'}\,\partial\overline{v_i}/\partial x_j + \overline{v_3' T'}(g/\overline{T}),$$
$$N = -\overline{v_j' T'}\,\partial\overline{T}/\partial x_j. \qquad (6)$$

In order to present ε and N as functions of derivatives of the mean hydrodynamic fields, it is necessary to substitute in Eq. (6) the indicated statistical moments for their semiempirical representations from Eqs. (1) or (2).

However, for an arbitrary anisotropic boundary layer, which is of the greatest interest, the applicability of both hypotheses (1) and (2) is limited. The hypothesis (1), in which K_{ij} and K_{Tij} are to be considered different and not isotropic, is applicable to description of an arbitrary layer, but it is characterized by uncertainty of K_{ij} and K_{Tij} elements. Therefore, the expressions resulted from Eq. (6) can be a basis for the experimental studying of K_{ij} and K_{Tij} through measuring other quantities in these expressions. The hypothesis (2) is more detailed, but its application assumes a constancy of

the turbulent characteristics (V_*, T_*, L) throughout the layer and the presence of approximately even underlying surface.

At the same time, in any boundary layer the underlying surface can be considered the approximately even in quite small vicinity of every point (locally). Hence, it is possible to assume that in an arbitrary anisotropic boundary layer (including also a layer above the mountain relief) in some small vicinity of every observation point, the applicability conditions for the weakly anisotropic boundary layer of turbulent diffusion (2)–(4) (approximately even surface) are locally realized. Then, according to Eqs. (2)–(4), in the vicinity of every observation point in the layer, the variations of turbulent characteristics will be mainly caused, like in an isotropic layer, by variation of three independent parameters V_*, T_*, $\overline{T}$.

Using Eqs. (3) and (4), the indicated parameters can be converted into other three independent parameters ζ, V_*, T_* (with inclusion in their composition of the Monin–Obukhov number). The Monin–Obukhov number as a stratification parameter, takes into account the structure variations of the external energy influx then going into the turbulence energy, and, hence, is a convenient characteristic. The independent quantities ζ, V_*, and T_* are the functions of the radius-vector $\boldsymbol{r}$ of the observation point. If to choose in a boundary layer a set of observation points in such a way that when going from one point to another (along a certain trajectory with the arc length $s(\boldsymbol{r})$) the number $\zeta(\boldsymbol{r})$ changes monotonically, then after the change of independent variables $s(\boldsymbol{r}) \to \zeta(\boldsymbol{r})$ it is possible to consider the dependences $V_*(\zeta(\boldsymbol{r}))$, $T_*(\zeta(\boldsymbol{r}))$. Note that if the mean temperature varies weakly in the boundary layer, then there are two independent parameters V_* and T_* instead of three ones, which, in turn, can be substituted for ζ and V_* (or for ζ and T_*). Then, along the trajectory, where $\zeta(r)$ is monotonic, $V_*(\zeta(r))$ [in this case $T_*(\zeta(r))$ depends on $V_*(\zeta(r))$], or $T_*(\zeta(\boldsymbol{r}))$ [in this case $V_*(\zeta(\boldsymbol{r}))$ depends on $T_*(\zeta(\boldsymbol{r}))$] can be considered. Thus, if two functions $V_*(\zeta)$ and $T_*(\zeta)$ are known along the pointed trajectory (one of them is sufficient at $\overline{T} \approx$ const), then the Monin–Obukhov number ζ becomes the only universal parameter determining turbulence characteristics in a weakly anisotropic layer.

It follows from our measurements obtained in a mountain boundary layer (see below, Section 2, item 2.6) that the supposition of the local weak anisotropy of an arbitrary layer is true at a good accuracy. An arbitrary boundary layer, hence, can be considered as the locally weakly anisotropic. In an arbitrary anisotropic boundary layer all statistical characteristics of turbulence become functions of the Monin–Obukhov number, and some its value corresponds to every point in the layer.

According to the accepted assumption of the local weak anisotropy a semiempirical hypothesis (2) must be used in expression (6), and instead of K and K_T we use their representations from Eqs. (3) corresponding to the isotropic boundary layer ($K = æV_*z/\varphi(\zeta)$, $K_T = \alpha K$). Then it follows from Eqs. (2) (further, the bar above mean values of hydrodynamic fields is omitted):

$$V_*^2 = -\overline{v_1'v_3'} = KD^{\mathrm{V}},\ D^{\mathrm{V}} = \partial v_1/\partial x_3 + \partial v_3/\partial x_1, \quad (7)$$

$$\alpha æ V_* T_* = -\overline{v_3'T'} = K_T D^{\mathrm{T}},$$

$$D^{\mathrm{T}} = \beta_{31}\partial T/\partial x_1 + \beta_{32}\partial T/\partial x_2 + \beta_{33}\partial T/\partial x_3.$$

The immediate experimental testing of relations (7) in the mountain anisotropic boundary layer (see below, Figs. 19 and 20) has shown, that the left part of these relations satisfactorily coincides with the right part.

Substituting into Eq. (6) the semiempirical expressions (2), taking into account Eqs. (7) and the incompressibility condition, we obtain

$$\varepsilon = V_*^3 æ^{-1} z^{-1}[\varphi(\zeta) + \varphi_{\mathrm{V}}(\zeta) - \zeta], \quad (8)$$

$$\varphi_{\mathrm{V}}(\zeta) = æ^2 z^2 V_*^{-2} \varphi(\zeta)^{-1}\,[\Phi_{12}^2 + \Phi_{23}^2 + (1/2)\sum_{\mathrm{i}} \Phi_{\mathrm{ii}}^2],$$

$$\Phi_{\mathrm{ij}} = \partial v_{\mathrm{i}}/\partial x_{\mathrm{j}} + \partial v_{\mathrm{j}}/\partial x_{\mathrm{i}}, \quad (8a)$$

$$N = \alpha æ V_* T_*^2 z^{-1}[\varphi(\zeta) + \varphi_{\mathrm{T}}(\zeta)], \quad (9)$$

$$\varphi_{\mathrm{T}}(\zeta) = T_*^{-1} z[(\beta_{13} - \beta_{31})(\partial T/\partial x_1) +$$

$$+ (\beta_{23} - \beta_{32})(\partial T/\partial x_2)] + T_*^{-2} z^2 \varphi(\zeta)^{-1}[\eta_1(\partial T/\partial x_1)^2 +$$

$$+ \eta_2(\partial T/\partial x_2)^2 + \eta_{12}(\partial T/\partial x_1)(\partial T/\partial x_2)], \quad (9a)$$

$$\eta_1 = \beta_{11} - \beta_{13}\beta_{31},\ \eta_2 = \beta_{22} - \beta_{23}\beta_{32},$$

$$\eta_{12} = \beta_{12} + \beta_{21} - \beta_{23}\beta_{31} - \beta_{13}\beta_{32},\ \beta_{33} = 1.$$

Comparing Eqs. (8) and (9) for ε and N, obtained for the anisotropic boundary layer, with expressions for ε and N in an isotropic layer,[1,3] it is easily to see, that anisotropic ε and N differ from isotropic ones only by the presence of functions $\varphi_{\mathrm{V}}(\zeta)$ (for ε) and $\varphi_{\mathrm{T}}(\zeta)$ (for N). These functions are added to the similarity function $\varphi(\zeta)$. Since $\varphi_{\mathrm{V}}(\zeta)$ and $\varphi_{\mathrm{T}}(\zeta)$ are the characteristics of an anisotropic layer, they can be called the functions of anisotropy. According to Eq. (8), $\varphi_{\mathrm{V}}(\zeta)$ characterizes the rate of energy dissipation, therefore, it can be termed the anisotropy power function. Function $\varphi_{\mathrm{T}}(\zeta)$ in Eq. (9) characterizes the dissipation rate of temperature fluctuations; therefore, it can be termed the anisotropy temperature function.

In expressions (8) and (9) it is still necessary to pass to the coordinate system, in which the axis $ox_1 = ox$ is directed along the mean velocity of a horizontal wind. In such a system, the transversal horizontal component of the mean velocity is absent ($v_2 = 0$ along the axis $ox_2 = oy$) and the mean velocity vector $\mathbf{v}$ has components $\mathbf{v} = (v_1, 0, v_3) = (u, 0, w)$. This fact usually allows one to think, that in a certain local vicinity of every point the transversal derivatives (along ox_2) are small in comparison with longitudinal (along ox_1) and vertical (along $ox_3 = oz$) derivatives. Such assumptions

correspond to the frequently accepted conditions of the tensor Φ_{ij} symmetry in the semiempirical hypothesis (1): $\Phi_{21} = \Phi_{12} = \Phi_{32} = \Phi_{23} = 0$. Hence, $\varphi_V(\zeta)$ in Eq. (8a) can be rewritten as

$$\varphi_V(\zeta) = 2æ^2 z^2 V_*^{-2} \varphi(\zeta)^{-1} [(\partial v_1/\partial x_1)^2 + (\partial v_3/\partial x_3)^2]. \quad (8b)$$

If to take into account the incompressibility condition $\partial v_n/\partial x_n = 0$, then from Eq. (8b) we obtain

$$\varphi_V(\zeta) = 4æ^2 z^2 V_*^{-2} \varphi(\zeta)^{-1} (\partial v_1/\partial x_1)^2 \quad (8c)$$

or

$$\varphi_V(\zeta) = 4æ^2 z^2 V_*^{-2} \varphi(\zeta)^{-1} (\partial v_3/\partial x_3)^2.$$

These expressions must be true simultaneously. At the same time, according to Eq. (2)

$$2K(\partial v_1/\partial x_1) = \tau_1, \ \tau_1 = \overline{v'_n v'_n}/3 - \overline{v'_1 v'_1};$$

$$2K(\partial v_3/\partial x_3) = \tau_3, \ \tau_3 = \overline{v'_n v'_n}/3 - \overline{v'_3 v'_3}.$$

Expressing the derivatives through τ_1, τ_3, K and substituting them into Eq. (8c), we found

$$\varphi_V(\zeta) = V_*^{-4} \varphi(\zeta) \tau_1^2, \ \varphi_V(\zeta) = V_*^{-4} \varphi(\zeta) \tau_3^2. \quad (8d)$$

The requirement of simultaneous fulfilling of equations (8d) corresponds to supposition on isotropy of K_{ij} in Eq. (2). A comparison of experimental and theoretical (calculated by Eq. (8b)) values of $\varphi_V(\zeta)$ for an anisotropic boundary layer will be conducted further in Section 2, but a preliminary estimate of the error in the supposition can be made just now based on measurements of turbulent pulsations of velocity components.

Measuring results on the root-mean-square deviations of the turbulent fluctuations of the velocity components in the mountain anisotropic boundary layer in a wide range of the Monin–Obukhov number values (from stable to super unstable local temperature stratifications, $-581 \le \zeta \le 0.3$, see below, Section 2) are presented in Fig. 2.

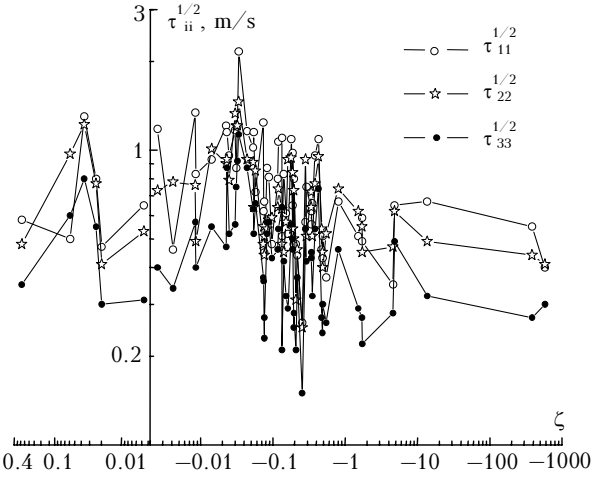

Fig. 2. Root-mean-square deviations of the wind velocity fluctuations for all measuring sessions $\tau_{ii}^{1/2} = \overline{v'_i v'_i}^{1/2}$ (i = 1, 2, 3); $\tau_{11} = \overline{v'_1 v'_1}$, $\tau_{22} = \overline{v'_2 v'_2}$, $\tau_{33} = \overline{v'_3 v'_3}$.

As is seen, the proportions between pulsations of different components hold, on the average, in the entire range of ζ variation. Therefore, averaging the experimental data over the entire ζ range, we obtain (in $[m^2/s^2]$)

$$<\overline{v'_1 v'_1}> = 0.60, \ <\overline{v'_2 v'_2}> = 0.47, \ <\overline{v'_3 v'_3}> = 0.20,$$

that corresponds to $<\tau_1> = -0.17$, $<\tau_3> = 0.22$. Then deviations of τ_1^2 and τ_3^2 values (in both sides) in Eq. (8d) from their total mean do not exceed 25%. Hence, the inherent measurement error for $\varphi_V(\zeta)$, arising from the assumption of K_{ij} isotropy in Eq. (2), does not exceed 25% as well. The experience in measuring turbulence characteristics in atmosphere shows such error to be quite satisfactory.

Note that since measurements of derivatives with respect to hydrodynamic fields in atmosphere are usually accompanied by significant errors, the relation (8b), smoothing the measuring errors, is better suited to measurements of the anisotropy power function $\varphi_V(\zeta)$.

Expression (9a) for the anisotropy temperature function $\varphi_T(\zeta)$ also can be simplified, using symmetry equalities of K_{Tij} in Eq. (3) ($\beta_{12} = \beta_{21} = \beta_{23} = \beta_{32} = 0$):

$$\varphi_T(\zeta) = (\beta_{13} - \beta_{31}) T_*^{-1} z (\partial T/\partial x_1) + T_*^{-2} z^2 \varphi(\zeta)^{-1} \times$$
$$\times [(\beta_{11} - \beta_{13}\beta_{31}) (\partial T/\partial x_1)^2 + \beta_{22} (\partial T/\partial x_2)^2]. \quad (9b)$$

In the coordinate system with the axis ox_1 directed along the mean velocity of the horizontal wind, it follows from Eq. (9b)

$$\varphi_T(\zeta) = (\beta_{13} - \beta_{31}) T_*^{-1} z (\partial T/\partial x_1) +$$
$$+ (\beta_{11} - \beta_{13}\beta_{31}) T_*^{-2} z^2 \varphi(\zeta)^{-1} (\partial T/\partial x_1)^2. \quad (9c)$$

Thus, as is seen from Eqs. (8c) and (9c), the assumption of the local weak anisotropy of an arbitrary boundary layer reduces the calculation of $\varphi_V(\zeta)$ and $\varphi_T(\zeta)$ (as well as the dissipation rates ε and N) to determination of the turbulence scales V_* and T_*, the Monin–Obukhov number ζ, and two longitudinal derivatives $\partial T/\partial x_1$, $\partial v_1/\partial x_1$. In the isotropic boundary layer, the longitudinal derivatives and v_3 are zero, hence, $\varphi_V(\zeta) = \varphi_T(\zeta) = 0$.

2. Experimental testing of semiempirical hypotheses in the anisotropic boundary layer

In Section 1 of this work, the assumption of local weak anisotropy of an arbitrary boundary layer has been made. Based on this assumption and using semiempirical hypotheses of the turbulence theory, theoretical expressions for fundamental turbulence characteristics (average dissipation rates ε and N) for the anisotropic boundary layer were obtained.

In the given Section, the results of experimental testing of the obtained expressions for dissipation rates ε and N, which, according to Eqs. (8) and (9), are reduced to results of the experimental testing of theoretical representations for the power and

temperature anisotropy functions $\varphi_V(\zeta)$ and $\varphi_T(\zeta)$ are described. It is shown, that a satisfactory agreement between theory and experiment takes place.

Turbulent characteristics were measured in the atmospheric boundary layer in mountains (the Baikal astrophysical observatory of the Institute of Solar-Terrestrial Physics of the Siberian Branch of the Russian Academy of Science, the settlement Listvyanka in Irkutsk Region, coast of Lake Baikal). The measurement region included flanks and a peak of the mountain on which the Big Solar Vacuum Telescope (BSVT) is situated. Because this mountain has no own name, for brevity we call it the BSVT-mountain. The mountain height above the sea level is 680 m. The total length of the measuring path is about 3 km. Characteristics of the atmospheric turbulence were fixed basically at a height of 2.7 m from the underlying surface. In total, 5 observation sessions with various types of the regional meteosituation were carried out. Measurements were made in 73 different points of the path. The time of measurements was from October 12 to October 28, 2002.

2.1. Equipment

The METEO-2M mobile ultrasonic meteosystem, developed at the Institute of Atmospheric Optics SB RAS was used in the measurements. The device measures the sound velocity having passed between two sensors of its measuring head. The measuring head is represented by two identical metal rings of 12 cm radius, located crosswise to each other with a common center. In the point of crossing, the rings are attached to the top of the cylindrical foundation of about 3 cm radius and 20 cm length. The ultrasonic sensors are located along the perimeters of each ring. The block for measuring pressure and humidity (a cylinder of about 3 cm in radius and 6 cm in length) is attached to the bottom side of the foundation at 15 cm distance from its axis. The measuring head is established on a metal mast (diameter of 3.5 cm) of a variable length.

Four measuring channels "source–receiver" are involved in the system. Measurement frequency is determined by the velocity of the sound propagation in air and the equipment reliability. For each channel, the reading frequency is 10 Hz. A two-level procedure is used in the processing of measurement results. The preprocessing mainly consists in averaging high-frequency measurements (at a 10 Hz frequency), which proceeds in the measuring head's processor and serves to improve the equipment reliability. The final processing is performed at a portable computer of "Note Book" type. The averaging time is set by the observer and, depending on the measuring mode, can vary from 1 minute to several days.

The meteosystem records 89 parameters (at a height of the measuring head's center), stores the measuring results simultaneously as a binary file and a text report. The main measurable characteristics are: mean air temperature (°C); mean components of the wind vector (m/s), including modulus of the averaged velocity vector (m/s), modulus (m/s) and direction (deg) of the averaged horizontal velocity vector, modulus (m/s) and direction (upward-downward) of the averaged vertical component of the velocity vector; absolute (g/m^3) and relative (%) air humidity; atmospheric pressure (mm Hg); the structural characteristics of the temperature fluctuations C_T^2 ($deg^2 \cdot cm^{-2/3}$), longitudinal component of the wind velocity C_V^2 ($(m/s)^2 \cdot cm^{-2/3}$), an acoustic index of refraction $C_{n,a}^2$ ($m^{-2/3}$), and optical index of refraction C_n^2 ($cm^{-2/3}$). Besides, the system records the root-mean-square deviations of temperature, velocity vector components and directions; fixes coefficients of correlation, asymmetry, and excess (between and for basic measurable parameters); measures the total energy of turbulent motions (m^2/s^2), the moments of momentum and heat flux (m^2/s^2), vertical flux of momentum and heat; dissipation rates of the kinetic energy ε (m^2/s^2) and the temperature fluctuations N (deg^2/s); the turbulent scales of the Monin–Obukhov scale L (m), temperature T_* (°C), and wind velocity V_* (m/s); the Monin–Obukhov number ζ ($\zeta = z/L$), and other characteristics. The system records also the frequency spectra of temperature fluctuations and the vector components of wind velocity.

The system has passed a full set of metrological tests, including tests in altitude/temperature and humidity/temperature chambers, as well as in wind tunnel. The systematic measurement errors were determined by the device calibration, and for basic averaged parameters are 0.3°C (for temperature) and 0.15 m/s (for vector components of wind velocity). However, the device sensitivity (its capability to distinguish different measurements at the same systematic error during long-time observations) is essentially less and for random values makes up 0.002°C and 0.03 m/s for temperature and vector components of wind velocity, respectively. Systematic error in measuring the pressure is 2 mm Hg (at a sensitivity of 0.01 mm Hg), in measuring the relative humidity it is 0.1%.

The upper boundary of the instrument transmission band is determined by the frequency of generating results and makes up 10 Hz. The averaging arised because of the device time constant leads to cutting high frequencies in the spatial turbulence spectrum. Therefore, the equipment is not sensitive to turbulent heterogeneities, which sizes, for example, at a mean wind velocity of 1 m/s are less than 10 cm. Such a time constant limits possibilities of studying small-scale turbulence components experimentally. At the same time, it practically does not affect the accuracy in measuring random characteristics of meteofields. Thus, the direct measurements of the turbulence spectra show that at recording random temperature and wind velocity the

error brought by the device time constant, usually does not exceed 1%. This is due to insignificant contribution of the cut portion of the spectrum in the total energy of fluctuations.

As is generally known,[1,3] the averaging time in measurements of the turbulent parameters should be chosen for the condition, that the length scale of the averaged turbulent flow (mean wind velocity multiplied by the averaging time) essentially exceeds the outer scale of turbulence in the direction of the mean flow (or, that is the same, the averaging time should essentially exceed the characteristic time scale of correlation of the investigated field). Then the temporal means are statistically stable. Measurements in the ground layer above some surface are usually conducted at the averaging time not less than 100 s (Refs. 1 and 3). The length scale for wind velocity of 1–10 m/s corresponding to this time is 0.1–1 km and exceeds the outer scale of turbulence. In case of uneven surface, the longitudinal outer scale of turbulence in the ground layer is, obviously, determined by typical distance between different surface unevennesses or inhomogeneities. For a mountain relief with inhomogeneous surface, such a near-surface distance is insignificant and can be estimated by tens of meters. Hence, measurements in the ground layer above uneven surface can be carried out with averaging time of about 100 s. In this work, when recording turbulence parameters in one point, the averaging time is 2 minutes.

The relative error in measuring structural characteristics is determined, first of all, by the device sensitivity and decreases with the increase of mean wind velocity, averaging time, and values of structural characteristics. So, for example, in conditions of relatively weak turbulence ($C_n^2 = 5 \cdot 10^{-16}$ cm$^{-2/3}$) at an averaging time of 2 minutes and a mean wind velocity of 0.5–10 m/s the relative error in measuring C_n^2 is within 0.4–14% (0.4, 7, 14% for wind velocity of 10; 1; 0.5 m/s, respectively). Characteristics C_T^2 and C_V^2 are measured with the same errors. Dissipation rates ε and N are measured based on relations (5) (Kolmogorov–Obukhov law). Hence, the relative error in measuring ε (N) practically is a sum of errors of C_V^2 and the Kolmogorov constant C (C_T^2 and the Obukhov constant C_θ).

After conducting field measurements, the control testing of the meteosystem has been made, which has confirmed the reliability of the obtained data.

2.2. Requirements to the duration of observation sessions

As is well-known,[1,3,6] when measuring atmospheric turbulence parameters in an isotropic boundary layer (plane-parallel flows above even, homogeneous, and equally heated surface), it is required that the observation session was carried out approximately in the same regional meteosituation with some established mode of the turbulent motions. During field measurements, it is necessary to exclude the influence of daily variations and noticeable changes in the overcast regime and, in particular, variable overlaps of sun by clouds. Then stratification parameters responsible for turbulent meteosituation above the territory of interest (for example, the Monin–Obukhov number or the Richardson number) are approximately constant and the measured time-average values are stable (they depend only on the type of the regional meteosituation).

The requirement of the constant regional meteosituation is not principal for measurements in the mountain anisotropic boundary layer (according to results from Section 1), where all turbulence characteristics become functions of the Monin–Obukhov number, and a particular number value corresponds to every point in the layer. However, to be sure, a series of measuring sessions must be conducted with approximately constant regional meteosituation in each of them. From comparison of results, it is possible to find the degree of influence of the meteosituation type.

Besides, as follows from Eqs. (7), (8b), (9c), to compare the experiment and theory, it is necessary to measure various spatial derivatives of meteofields. At the same time, the approximation of derivatives by difference relations usually leads to significant errors. They can be essentially reduced when using data obtained in stable meteosituations.

Thus, to carry out necessary measurements, a series of sessions must be conducted with approximately constant meteosituation in each.

Since the known stratification parameters (the Monin–Obukhov number or the Richardson number) are different in a mountain boundary layer, they can not serve indicators of some general meteosituation in a mountain region. Apparently, such indicators are stratification parameters averaged over many surface points. However, during measurements, such efficient parameters are not known in advance.

In this connection, the meteosituation in our measurements was estimated, first of all, from the stability of the solar radiation intensity, as well as from the amount and motion of clouds. During the whole measuring session, the Sun must be closed or opened by clouds without periodical changes of the situation. In October, such stability in the region of the Baikal astrophysical observatory is usually observed in the second half of the day, beginning from 1–2 p.m. of the local time. Durations of the highly stable meteosituation for the open Sun (overcast is insignificant and, as a rule, near the horizon) and for the closed Sun (complete and dense overcast) are approximately identical: from 3 to 5–7 hours. However, unstable meteosituations, characterized by significant broken (or complete, but not dense) overcast (mostly in the first half of the day) are more frequent. The duration of the open Sun at the broken overcast is usually less than 1–1.5 hours.

Except for the qualitative control for the overcast state, the dynamics of the regional turbulent

meteosituation for some time interval can be estimated from measurements of the near-surface values of C_n^2 (or C_T^2 and C_V^2), at one point. The preliminary measurements conducted in the second half of the day at the same place have shown that in case of constantly open Sun at approximately identical amount of clouds the near-surface values of C_n^2 can vary (decrease) 1.5–2 times for 2–3 hours because of the daily solar motion (the result varies depending on a geographical position of the measuring point). At complete and dense overcast, the same variation occurs for a greater time, approximately, for 2–4 hours. The variation of C_n^2 is stronger in case of instable meteosituation, when the Sun is periodically opened or covered by clouds, or the density of clouds covering the Sun varies.

Obviously, the duration of observation sessions should be minimized. Once the recording of turbulent characteristics at one point proceeds 5–7 minutes, including a two-minute measuring time, the time for activation and deactivation of the equipment, and the time necessary for going from one observation point to another, then at a highly stable meteosituation of duration no less than 3 hours, about 30 points can be recorded without an appreciable error for a measuring session. At a low-stable meteosituation, the measuring session should not exceed 1–1.5 hours.

Five measuring sessions were carried out for all time of the expedition (from October 12, to October 28, 2002). The first session was carried out on October 17 in the first half of the day (sunny morning, wind of 1–2 m/s, temperature of 1–0°C, humidity of 49–61%). The second one was conducted on October, 17 in the second half of the day (complete overcast, white haze, wind of 0.3–5 m/s, temperature of 0.4–+1.7°C, humidity of 46–62%), the third one – on October 18 in the second half of the day (sunny day, wind of 1–8 m/s, temperature of 0–+3.7°C, humidity of 35–63%), the fourth and the fifth sessions were conducted on October 22 in the second half of the day (complete overcast, wind of 1–3 m/s, temperature of 0.9–+1.1°C, humidity of 37–57%). In first three sessions measurements were carried out along the entire path, and covered large areas; in the fourth and the fifth sessions – only on the peak of the BSVT-mountain, but with a better resolution. During the fifth session, high-altitude measurements in the low 5-meter layer were carried out. During the first and the third sessions, the weather was clear and sunny with similar stable meteosituations; during the second, fourth, and fifth sessions the sun was covered with clouds.

2.3. Characterization of the measuring path

The measuring path was chosen so that to combine recording of turbulence parameters with recording of near-surface fields of C_n^2. The values of C_n^2 were necessary for forecasting BSVT image quality. Therefore, the measuring path included flanks and the peak of the BSVT-mountain.

According to the purpose of measurements, the path along the BSVT-mountain flanks should fall in the observation sector of the BSVT, i.e., it had to go along the projection of the optical path to the underlying surface strictly southward from the telescope, which was oriented from north to south. However, because of the necessity to use an automobile during measurements, the path had to be passable. Therefore, the actual directions of the route along the mountain flanks and canyons sometimes differed approximately by 20–35° from the north–south direction.

All path was divided into two segments *HO* and *OB* (Fig. 3). The point *H* was located at the field office of the BSVT administration. The *HO* segment passed along the mountain flank neighboring to the BSVT-mountain. The point *O* was the conditionally junction point, where the canyon between two mountains ended.

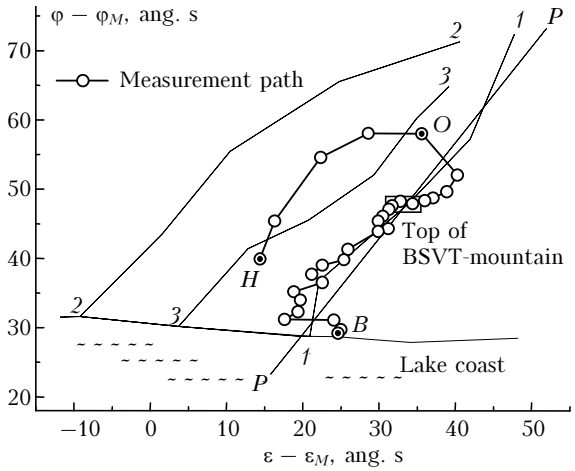

Fig. 3. Scheme of the measurement path: φ is the latitude, ε is the longitude; (φ_M, ε_M) are the latitude and longitude of the referent point *M*. The path includes the *HO*, *OB*, *HOB* routes. Orientations of mountain ridges and canyons: (*11*) the ridge of the BSVT-mountain; (*22*) the neighboring mountain's ridge; (*33*) the canyon; (*PP*) the reference vertical plane.

Beginning from the point *O*, the path goes along the northern (back) flank of BSVT-mountain, rises to the peak and then goes down along the south (face) flank to Lake Baikal up to the point *B*, which is situated at the lake coast line close to water. All the coordinates in Fig. 3 are related to some reference point *M*, which is situated on the lake surface in several hundreds of meters from the coast near the point *B*.

When investigating the behavior of turbulence characteristics throughout the path (usually, at a height of 2.7 m above the surface), it is convenient to use the central earth angle α as an independent argument. Then the route segments corresponding to the observation sessions 1–3, are sewed together in one route *HOB*. One second in the angle α approximately corresponds to 31 m on the geoid

surface, therefore, when moving along the trajectory of the compound route, the central angle α increases. Sometimes, the route at the peak of the BSVT-mountain (the 4th session, with a more detailed resolution) is added to the *HOB* route (sessions 1–3). In coincident points (few in number) the values from only one observation session were taken.

The recorded altitude profile (relative to the sea level) of the measurement path is presented in Fig. 4. For comparison, the altitude profile of the path fragment *OB* is presented as well, each point of which is projected on the auxiliary reference vertical plane *PP*.

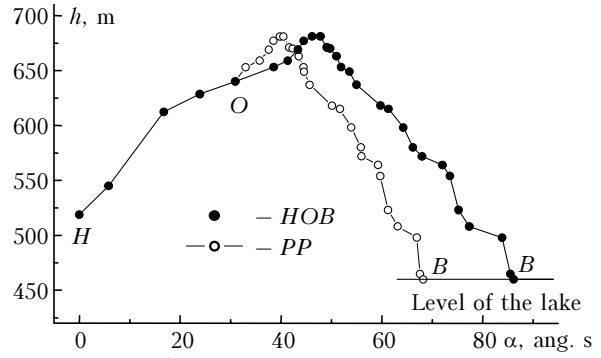

Fig. 4. An altitude profile of the measurement path: h is the height above the sea level, α is the central earth angle. Dark points correspond to the *HOB* route, light points – to the *OB* route along the reference plane *PP* (projections of route points *OB* on the *PP* plane).

This projection allows estimate how zigzag is the route, its maximal deviations from the fixed direction set by the *PP* plane, as well as deviations from the telescope orientation direction (north–south). As Fig. 4 shows, the actual altitude profile of the BSVT-mountain corresponding to the projection on the *PP* plane, is more steep than the profile along the measurement path.

Deviations of the altitude profile of the measurement path from the averaged altitude of BSVT-mountain profile are 5–10 m (both upwards and downwards). The underlying surface along the path is covered with rather thin (basically, pine) wood of 7–15 m height. Along some route legs the wood is absent, and the rocks covered with low grass are observed.

2.4. General measurement results of the turbulence characteristics in the mountain boundary layer

It is experimentally found that the turbulence in the mountain boundary layer is essentially anisotropic. Even at a stable regional meteosituation the structural characteristics C_T^2, C_V^2, C_n^2 can vary by more than 2 orders of magnitude depending on the position of the recording point. They can be significantly affected by surface areas with increased heat exchange and high thermal capacity (for example, the surface of Lake Baikal), where C_T^2, C_V^2, and C_n^2 are practically independent of the meteosituation type.

Large heterogeneities of relief and artificial cultures create stable rotary perturbations of airflows. Wind maps of the observation region are presented in Figs. 5 and 6. As is seen in Fig. 5, airflows at flanks of two parallel mountain ridges are directed to the canyon bottom. In similar meteosituations a stability of such flows is observed (see Fig. 5 near the point *O*).

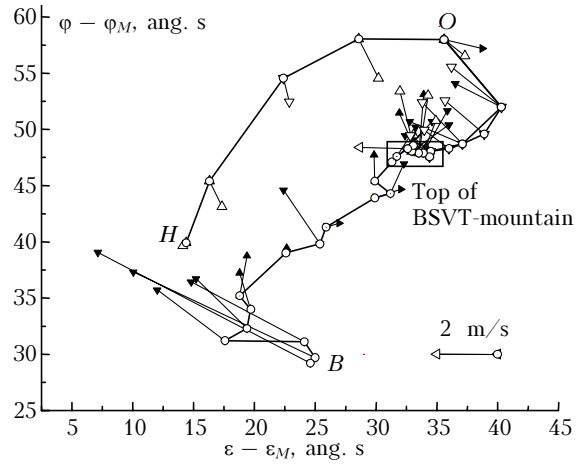

Fig. 5. Wind map of the measurement route at a constant meteosituation. Arrows with white triangles refer to the 1st session, arrows with black triangles – to the 3rd session. The measurement route is designated by the solid line (routes *HO*, *OB*, *HOB*).

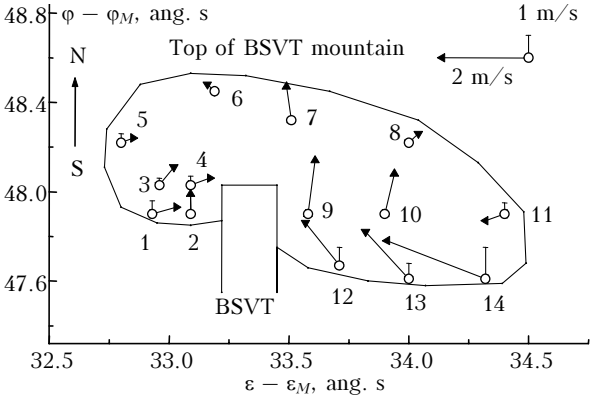

Fig. 6. Wind map of the BSVT-mountain peak (a 3D vector field of the mean wind at the mountain peak, on the platform near the BSVT, which border is shown by solid line): φ is the latitude, ε is the longitude, (φ_M, ε_M) are the latitude and the longitude of the reference point *M*. The 4th observation session, measurements at a height of 2.7 m from the underlying surface. Vertical straight lines near points show the magnitude of vertical component in the mean 3D-wind vector.

At the BSVT-mountain peak wind flows from the lake are reflected from the high (26 m) BSVT building and, as Fig. 6 shows, the stable rotary flows take place there, in particular, near points 8, 10, 11, and 14 (Fig. 6). Near centers of such vortex formations small values of the wind velocity vector,

an increased pressure, and a lowered humidity are observed.

Around the centers the local temperature stratification can vary from extremely unstable to stable. It is evident, for example, in Fig. 7, in which the recorded field of the Monin–Obukhov numbers ζ corresponds to a height of 2.7 m above the peak of the BSVT-mountain. Thus, the local superstrong unstable stratification (ζ = –388) in the same as in Fig. 6 point 8 is observed. However, nearby, in the point 11 (in several tens of meters from the point 8), the Monin–Obukhov number already corresponds to the local stable stratification (ζ = +0.3).

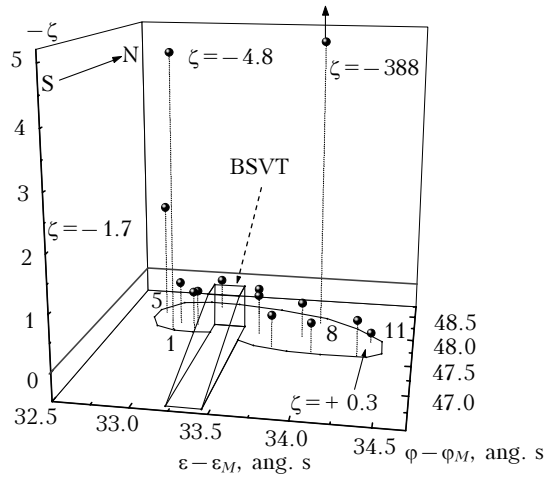

Fig. 7. The field of Monin–Obukhov number ζ values at the BSVT-mountain peak. The forth measurement session at a height of 2.7 m from the underlying surface. Separately, ζ values are shown strongly differing from stratification boundaries $|\zeta| = 0.05$; for other points: $-0.34 < \zeta < -0.05$.

As Fig. 8 shows, numbers ζ measured at the same height of 2.7 m vary in the same observation point as the regional meteosituation varies.

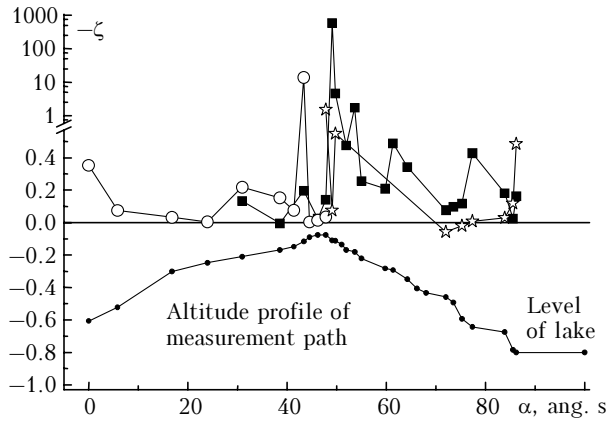

Fig. 8. The Monin–Obukhov number ζ in the measurement sessions 1–3: α is the central angle of earth. Measurements at a height of 2.7 m from the underlying surface. Light circles refer to session 1; asterisks – to session 2; dark squares – to session 3.

The fundamental turbulence characteristics vary essentially in the mountain boundary layer as well: mean dissipation rates of the kinetic energy ε (Fig. 9) and temperature N (Fig. 10), as well as the turbulent scales of temperature T_* (Fig. 11) and velocity V_* (Fig. 12).

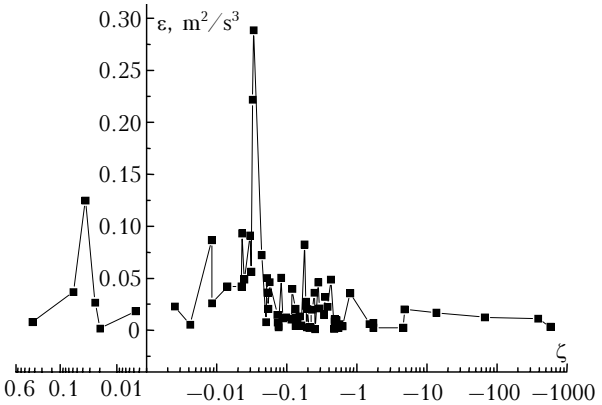

Fig. 9. Mean dissipation rate of the turbulence kinetic energy ε in a mountain boundary layer for all measuring sessions, depending on the Monin–Obukhov number ζ.

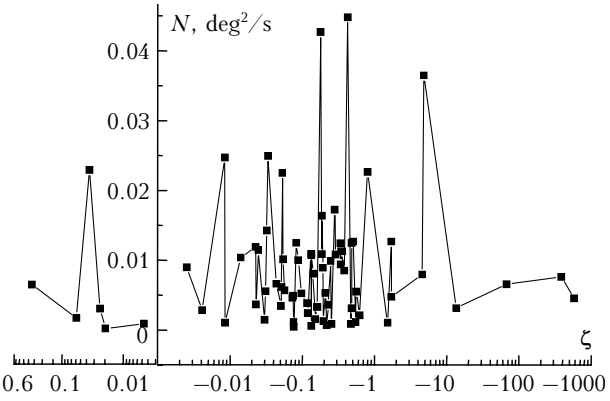

Fig. 10. Mean dissipation rate of temperature fluctuations N in a mountain boundary layer for all measuring sessions depending on the Monin–Obukhov number ζ.

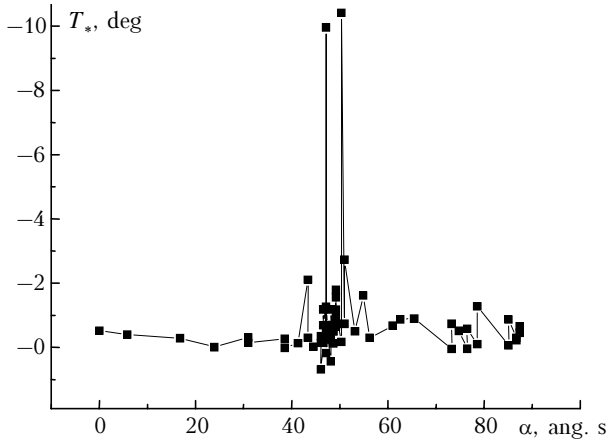

Fig. 11. Turbulent scale of the temperature field T^* in a mountain boundary layer for 1–4 measuring sessions, depending on the earth central angle α.

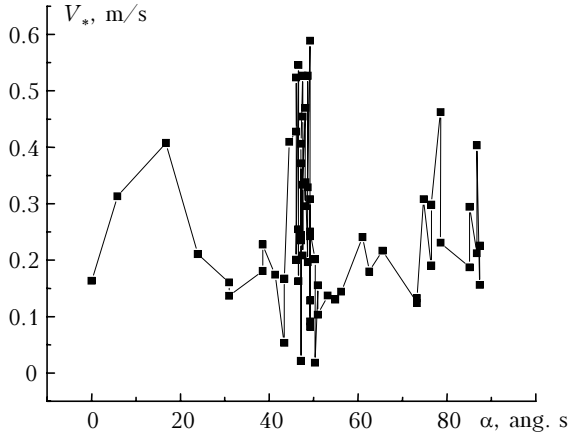

Fig. 12. Turbulent scale of the velocity V^* field in a mountain boundary layer for the 1–4 measuring sessions, depending on the earth central angle α.

The mean temperature T (°C) is also variable. The values of the Kolmogorov inner scale of turbulence l_0 were obtained, using the measured dissipation rates of ε, by the formula $l_0 = \nu^{3/4}\varepsilon^{-1/4}$, where $\nu = 1.3 \cdot 10^{-5}$ m^2/s is the air kinematic viscosity at 0°C. The l_0 values are in the range from 0.3 to 1.2 mm (mean of 0.64 mm). The Kolmogorov inner scale is inversely proportional to the intensity of airflow velocity fluctuations. The stronger are the velocity fluctuations increasing near large obstacles, the less is the scale.

2.5. Measurement results for hydrodynamic field derivatives

The experimental values of derivatives $\partial T/\partial z$, $\partial T/\partial x$, $\partial u/\partial z$, $\partial u/\partial x$, $\partial w/\partial z$, $\partial w/\partial x$ (mean velocity of horizontal wind is directed along ox axis, z is the height), necessary for comparison of the experiment with the theory, were found from the usual difference relations approximating the derivatives. For example, for the point $z = z_0$, located in the interval $z_1 < z_0 < z_2$, $(\partial T/\partial z)|_{z=z_0} \approx [T(z_2) - T(z_1)]/(z_2 - z_1)$. To decrease the approximation errors, data obtained in the same stable meteosituation (in one observation session) were used in the difference relations.

The vertical derivatives of mean temperature $\partial T/\partial z$ were found from T measurements at different altitude levels (the 5th session at the peak of the BSVT-mountain, only 9 points). The vertical derivatives of the longitudinal ($\partial u/\partial z$) and vertical ($\partial w/\partial z$) components of mean velocity, in addition to direct measurements at different altitude levels, were restored also from the measurements at one height ($z = 2.7$ m) in view of the fact that velocity components (u, w) are zero (the adhesion condition) on the earth surface.

The longitudinal derivatives of temperature and velocity components ($\partial T/\partial x$, $\partial u/\partial x$, $\partial w/\partial x$) were restored from the near-surface measurements at one height ($z = 2.7$ m). As the derivative approximation by the difference relations gives the least error at small distances between two selected points, some restrictions were imposed on the distances. Both vertical ($z_2 - z_1$) and horizontal ($x_2 - x_1$) distances should not exceed the sizes of the outer scale of turbulence in the vertical and longitudinal horizontal directions. As it follows from our measurements (see below Fig. 26), the vertical outer scale of turbulence in the ground layer can be estimated by meters and tens of meters. The longitudinal outer scale of turbulence is, obviously, determined by the typical distance between the surface unevennesses or inhomogeneities. For a mountain relief with the inhomogeneous surface such distance is insignificant and on the average makes up about 50 m.

Note that calculating the longitudinal derivatives, we actually find the derivative values along the measurement path, i.e., derivatives along the vector **s** direction, connecting two observation points. Then, for example, for mean temperature we obtain $dT/ds = \partial T/\partial x \cos(x, s) + \partial T/\partial y \cos(y, s)$, where (x, s), (y, s) are the angles between the ox, oy axes and the vector **s** direction. The direction ox of mean wind velocity (and the longitudinal component), as a rule, does not coincide with the vector **s** direction ($\cos(x, s) \neq 1$, $\cos(y, s) \neq 0$). In view of the fact that transversal derivatives to average wind velocity (with respect to y) are usually essentially less then the longitudinal ones (with respect to x), then we find the formula, allowing us to restore the longitudinal derivatives $\partial T/\partial x \approx (dT/ds)/\cos(x, s)$ for moderately large angles between directions ox and **s** ($|\cos(x, s)| \geq 0.4$).

The measuring results for the hydrodynamic field derivatives are presented in Figs. 13–16, and further also in Figs. 19 and 20.

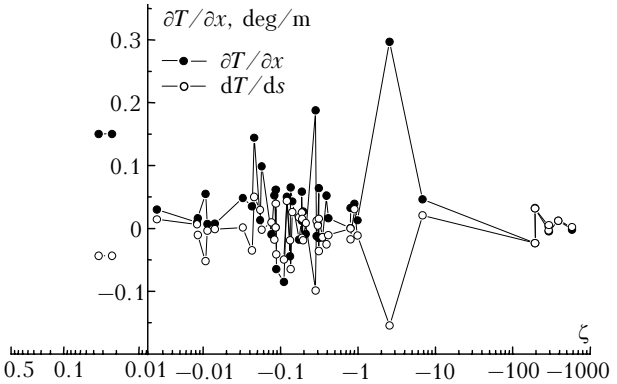

Fig. 13. Experimental values of $\partial T/\partial x$ in a mountain boundary layer for all measuring sessions. $\partial T/\partial x$ is the longitudinal (with respect to the direction ox of mean horizontal wind velocity) derivative of mean air temperature T, dT/ds is the derivative with respect to the trajectory of the measurement path.

Note that in the available similarity theory dimensionless quantities depending on dimensionless parameters are commonly used. Dimensional derivatives of hydrodynamic fields are not considered

independently. However, they are necessary to compare theory with experiment.

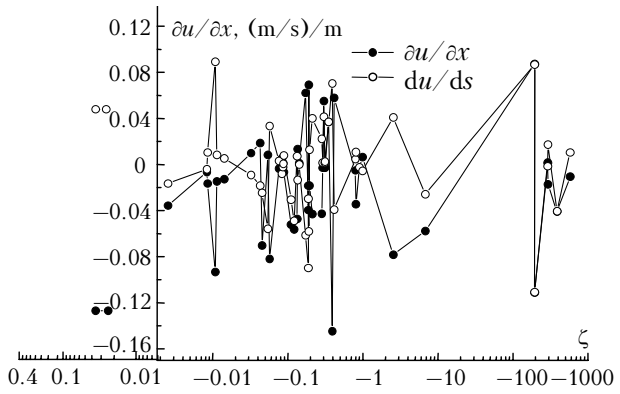

Fig. 14. Experimental values of $\partial u/\partial x$ in a mountain boundary layer for all measuring sessions. $\partial u/\partial x$ is the longitudinal (with respect to the ox direction of mean horizontal velocity) derivative of the longitudinal component u of mean wind velocity, du/ds is the derivative with respect to the trajectory of the measurement path.

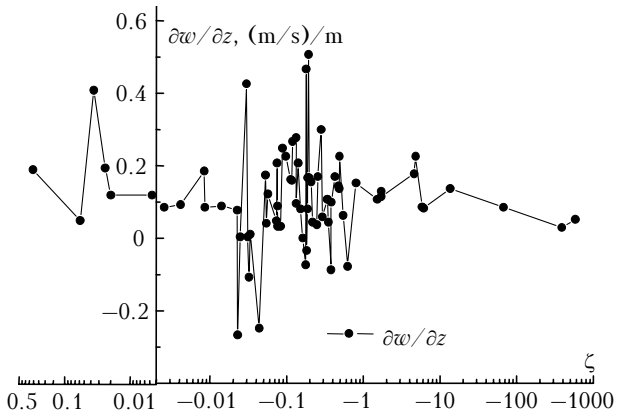

Fig. 15. Experimental values of $\partial w/\partial z$ in a mountain boundary layer for all measuring sessions. $\partial w/\partial z$ is the vertical (with respect to z) derivative of the vertical component w of the mean wind velocity.

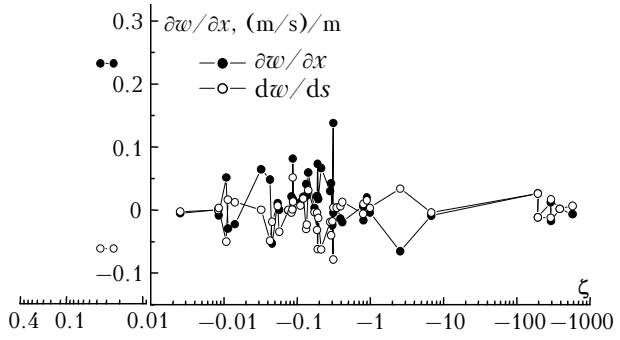

Fig. 16. Experimental values of $\partial w/\partial x$ in a mountain boundary layer for all measuring sessions. $\partial w/\partial x$ is the longitudinal (with respect to the ox direction) derivative of vertical component w of the mean wind velocity, dw/ds is the derivative with respect to the trajectory of the measurement path.

2.6. Anisotropy functions; the experimental testing of the mountain boundary layer for local weak anisotropy

According to results from Section 1, the requirement of constant regional meteosituation is not principal for measurements in a mountain anisotropic boundary layer. In such a boundary layer all turbulence characteristics become functions of the Monin–Obukhov number. The experimental results for scales of temperature T_* and velocity V_* for all observation sessions depending on the Monin–Obukhov number magnitude are presented in Figs. 17 and 18. In every session the regional meteosituation is described by a particular set of Monin–Obukhov numbers varying in the entire registered range: $-581 \le \zeta \le 0.3$. Joining all observation sessions in one, as Figs. 17 and 18 show, does not lead to a significant scatter of data.

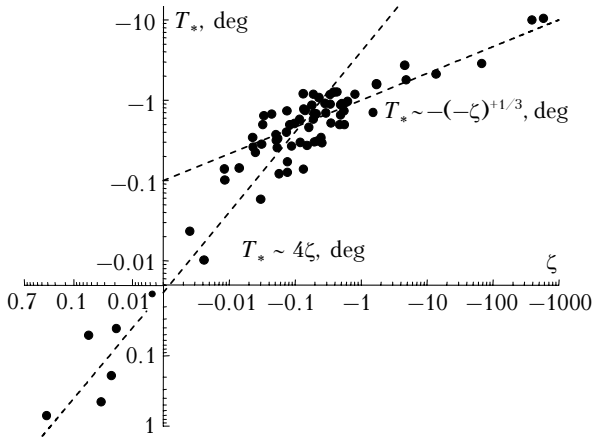

Fig. 17. Turbulent scale of the temperature field T^* in a mountain boundary layer for all measuring sessions, depending on the Monin–Obukhov number ζ.

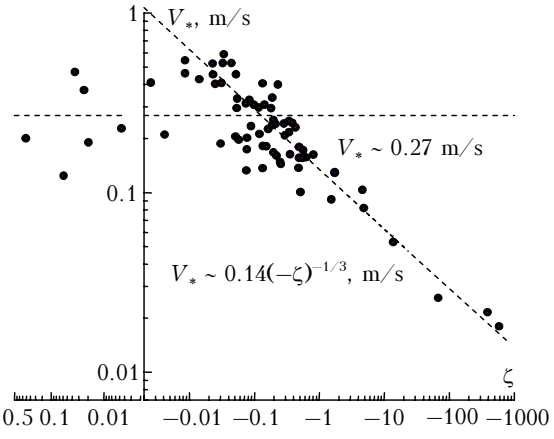

Fig. 18. Turbulent scale of the velocity field V_* in a mountain boundary layer for all measuring sessions, depending on the Monin–Obukhov number ζ.

All the data are stably grouped near certain smoothed dependences presented in Figs. 17 and 18. Some scattering of points observed in the stable

stratification area ($\zeta > +0.05$), uses to appear in the majority of measurements of various turbulent characteristics in atmosphere (according to works of different authors). A.S. Monin and A.M. Yaglom (Ref. 1) explain this by the turbulence intermittency in conditions of stability and, hence, by insufficiency of the usual averaging time. Thus, it follows from our measurements, that in the mountain boundary layer the experimental results, as functions of the Monin–Obukhov number, can be united independently of the regional meteosituation type (at least, for meteosituations observed for the time of our measurements).

Figures 19 and 20 present the results of comparison of the semiempirical theory with experiment for the functions

$$D^{\mathrm{T}} = \beta_{31}\partial T/\partial x_1 + \beta_{33}\partial T/\partial x_3$$

and

$$D^{\mathrm{V}} = \partial v_1/\partial x_3 + \partial v_3/\partial x_1$$

in a mountain boundary layer (see relations (7), in which at a mean wind velocity along the axis x_1, the transversal derivative $\partial T/\partial x_2$ can be neglected).

In case of isotropic boundary layer (when ζ is fixed, the longitudinal derivatives are absent and $D^{\mathrm{T}} = \partial T/\partial z$, $D^{\mathrm{V}} = \partial u/\partial z$), relations (7) are among the basic ones in the semiempirical turbulence theory (the similarity theory), which are reliably confirmed experimentally.[1,3] In an anisotropic layer all components of equalities (7) are functions of ζ varying at an arbitrary moving of the observation point. As is seen in Figs. 19 and 20, in a wide range of ζ variation the theory well coincides with the experiment. The account for longitudinal derivatives further improves the coincidence.

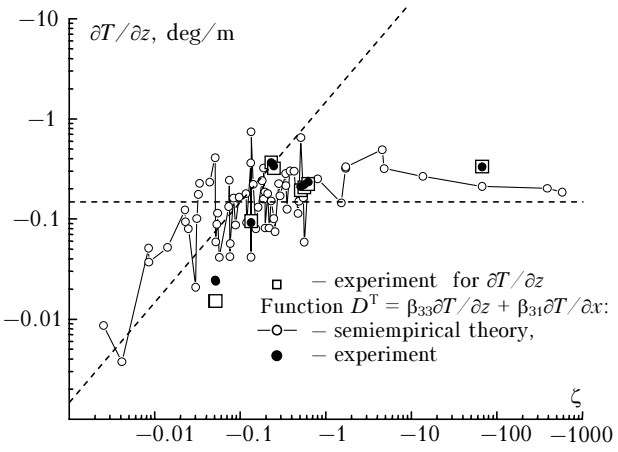

Fig. 19. Comparison of experimental and theoretical values of the vertical (with respect to z) derivative of the mean air temperature $\partial T/\partial z$ in a mountain boundary layer. Light squares denote experimental values of $\partial T/\partial z$ for the bottom 5-meter layer nearby the BSVT (the 5th observation session). Light and black circles refer, respectively, to theory and experiment for function D^{T} in Eqs. (7). The straight lines are asymptotics of D^{T} at $|\zeta| \to 0$ and $\zeta \to -\infty$.

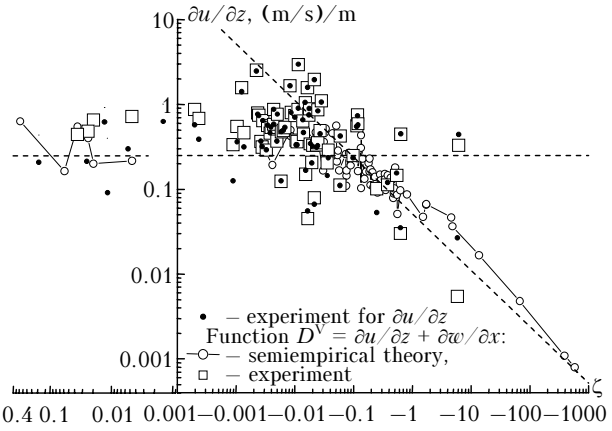

Fig. 20. Comparison of experimental and theoretical values of the vertical (with respect to z) derivative of the longitudinal component (u) of mean wind velocity $\partial u/\partial z$ in a mountain boundary layer. Black circles denote experimental values of $\partial u/\partial z$ in all observation sessions. White circles and white squares, respectively, refer to theory and experiment for the function D^{V} in Eqs. (7). Straight lines are asymptotics of D^{V} at $|\zeta| \to 0$ and $\zeta \to -\infty$.

Relations (7) and (3) show that functions D^{T} and D^{V} can be represented for the anisotropic layer as

$$D^{\mathrm{T}} = T_*(\zeta)\varphi(\zeta)/z,\ D^{\mathrm{V}} = V_*(\zeta)\ \varphi(\zeta)/(æz),$$

where $T_*(\zeta)$ and $V_*(\zeta)$ are functions of ζ (see Figs. 17 and 18). The same representations are also true for isotropic layer, but T_* and V_* in these formulas are constant.

As the measuring results demonstrate (see Figs. 19 and 20), there are local areas in the anisotropic layer, where the longitudinal derivatives in functions D^{T} and D^{V} can be neglected as compared to the vertical ones. This means that the isotropic layer mode is realized for D^{T} and D^{V} in such areas. A plane-parallel flow above an extended surface area can be considered simply an expansion of a certain small local area with the isotropic mode. Hence, in extended isotropic layers the constant T_* and V_* are not arbitrary, but, as is seen from theoretical representations for D^{T} and D^{V}, are determined by a particular magnitude of ζ.

The results of comparison of the semiempirical theory with the experiment for power and temperature anisotropy functions $\varphi_{\mathrm{V}}(\zeta)$, $\varphi_{\mathrm{T}}(\zeta)$ are presented in Figs. 21 and 22. Figures show their satisfactory coincidence. Theoretical values of these functions turn to be close to experimental ones in a wide range of variation of the Monin–Obukhov number (from stable to superstrong unstable local temperature stratification, $-581 \le \zeta \le 0.3$).

The anisotropy functions have maxima in different areas of ζ variation. If $\varphi_{\mathrm{T}}(\zeta)$ is concentrated mainly in the range $|\zeta| \lesssim 0.1$ then $\varphi_{\mathrm{V}}(\zeta)$ is in the range $-1 \gtrsim \zeta \gtrsim -1000$. Beyond these intervals both functions are close to zero, achieving in maxima values close to 1000. Despite of the low measurement accuracy of the hydrodynamic field derivatives, the coincidence is observed at the $\varphi_{\mathrm{V}}(\zeta)$ and $\varphi_{\mathrm{T}}(\zeta)$

variations more than by three orders of magnitude. Therefore, the coincidence cannot be a consequence of the experimental errors.

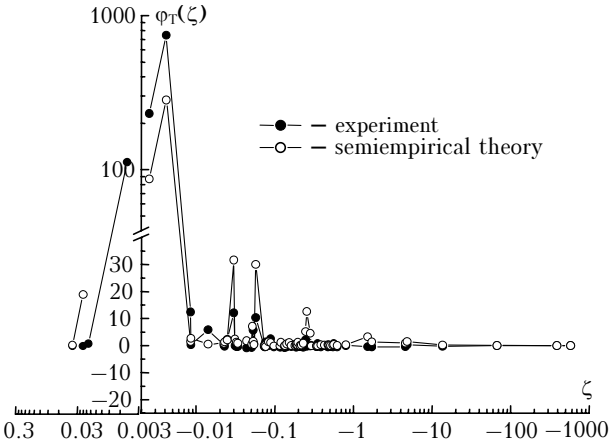

Fig. 21. Comparison of experimental and theoretical results for the anisotropy temperature function.

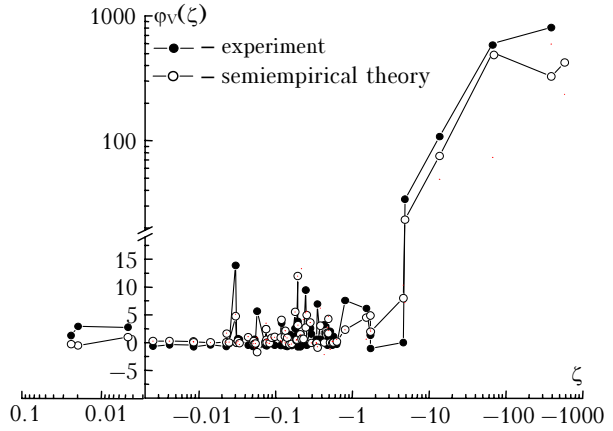

Fig. 22. Comparison of experimental and theoretical results for the anisotropy power function.

Since $\varphi_V(\zeta)$ and $\varphi_T(\zeta)$ determine the ε and N dissipation rates, it follows from Figs. 21 and 22 that the effect of anisotropic boundary layer on power (ε) and temperature (N) turbulence characteristics is essentially asymmetric. Appearance of maxima of the anisotropy function in different ranges of ζ variations is connected with corresponding behavior of $T_*(\zeta)$ and $V_*(\zeta)$ in these ranges. As is seen in Figs. 17 and 18, at small values of $|\zeta|$ ($|\zeta| \to 0$) $T_*(\zeta) \to 0$, but at large negative values of ζ ($\zeta \to -\infty$) $V_*(\zeta) \to 0$. Therefore, if the derivatives $\partial T/\partial x_1$ (at $|\zeta| \to 0$), $\partial v_1/\partial x_1$ or $\partial v_3/\partial x_3$ (at $\zeta \to -\infty$) in these ranges are limited, then, according to Eqs. (9c) and (8b) $\varphi_T(\zeta) \to \infty$ at $|\zeta| \to 0$ and $\varphi_V(\zeta) \to \infty$ at $\zeta \to -\infty$ (due to normalization on the scales T_* and V_*).

In the variation interval $-0.1 \gtrsim \zeta \gtrsim -1$, where both anisotropy functions are close to zero, expressions (8) and (9) for anisotropic dissipation rates ε and N coincide with expressions for isotropic rates of dissipation. Hence, in this interval of ζ values in the anisotropic boundary layer the isotropic layer mode is realized.

Thus, it follows from our measurements in a mountain boundary layer that the assumption of the local weak anisotropy of an arbitrary boundary layer is true with a good accuracy. The arbitrary boundary layer, hence, can be considered the locally weakly anisotropic. This means that the introduction of anisotropic functions $\varphi_T(\zeta)$ and $\varphi_V(\zeta)$ for isotropic dissipation rates into the similarity theory allows the theory expanding to an arbitrary anisotropic boundary layer.

3. Effective isotropic layer

It was shown in Section 2, that in a large interval of the Monin–Obukhov number variation ($-0.1 \gtrsim \zeta \gtrsim -1$) in a mountain boundary layer the isotropic layer mode is realized. The question of whether it is possible to substitute some arbitrary boundary layer for some effective isotropic boundary layer is of interest, because the positive answer would give a possibility to use simple semiempirical relations, valid in the isotropic layer, for description of the anisotropic layer.

As follows from formulas (8), (9), (8c) and (9c), in an arbitrary boundary layer the dissipation rates ε and N depend on five parameters: V_*, T_*, T, $\partial u/\partial x$, and $\partial T/\partial x$. Denote $\partial u/\partial x = V^X(\zeta)$, $\partial T/\partial x = T^X(\zeta)$ and consider that the form of functions $V^X(\zeta)$ and $T^X(\zeta)$ is well-known (experimental data for $\partial u/\partial x$, $\partial T/\partial x$ are presented in Figs. 13 and 14). Then relations for ε and N can be written as

$$\varepsilon = V_*^3 æ^{-1} z^{-1}[\varphi(\zeta) - \zeta + \varphi_V(\zeta,\ V_*,\ V^X(\zeta))],$$
$$N = \alpha æ V_*\, T_*^2\, z^{-1}[\varphi(\zeta) + \varphi_T(\zeta,\ T_*,\ T^X(\zeta))], \quad (10)$$
$$\zeta = z\alpha æ^2 g T_* V_*^{-2} T^{-1},$$

where all arguments in φ_V and φ_T are written out in the explicit form. Setting the parameter values for V_*, T_* and T in system (10), we find the values of the left parts of ε, N and ζ. Inverting the problem, it is possible to find V_*, T_* and T from the known ε, N and ζ.

The system of equations (10) corresponds to an anisotropic layer. If to set in Eqs. (10) $\varphi_V = 0$ and $\varphi_T = 0$, then the system (10) will describe an isotropic layer. Introducing new parameters $V_{*\mathrm{eff}}$, $T_{*\mathrm{eff}}$ and T_{eff} instead of V_*, T_* and T, we obtain

$$\varepsilon = V_{*\mathrm{eff}}^3 æ^{-1} z^{-1}[\varphi(\zeta) - \zeta],$$
$$N = \alpha æ V_{*\mathrm{eff}}\, T_{*\mathrm{eff}}^2\, z^{-1}\varphi(\zeta), \quad (11)$$
$$\zeta = z\alpha æ^2 g T_{*\mathrm{eff}}\, V_{*\mathrm{eff}}^{-2} T_{\mathrm{eff}}^{-1}.$$

Let us equate left parts of systems (10) and (11) to each other, that is equivalent to setting in Eqs. (11) magnitudes of ε, N and ζ corresponding to actual mountain layer. Solving the system of equations (11), we find the values of $V_{*\mathrm{eff}}$, $T_{*\mathrm{eff}}$ and T_{eff}, corresponding to an effective isotropic layer.

The problem can be simplified via considering relative variations of absolute temperature small and

supposing the temperature equal to its mean value over all observation sessions $T = T_{\text{eff}} = 273.7$ K ($\langle T\rangle = +0.5$°C, deviating in different sessions by 1–2°C). Then, having expressed one unknown from the third equation of system (11) through another and having substituted it into the first two equations, we obtain a system of two nonlinear equations with two unknowns $V_{*\text{eff}}$ and $T_{*\text{eff}}$.

The comparison of turbulent scales of temperature and velocity T_* and V_* for an anisotropic boundary layer with effective scales $T_{*\text{eff}}$ and $V_{*\text{eff}}$ for isotropic layer are presented in Figs. 23 and 24. It is seen that $T_{*\text{eff}}$ and $V_{*\text{eff}}$ are close to constants in a wide range of the Monin–Obukhov number variation ($-581 \le \zeta \le 0.3$). As is generally known, in an isotropic layer these scales should be constant. Based on data from Figs. 23 and 24, it is possible to draw a conclusion, that the anisotropic boundary layer can be substituted for an effective isotropic boundary layer.

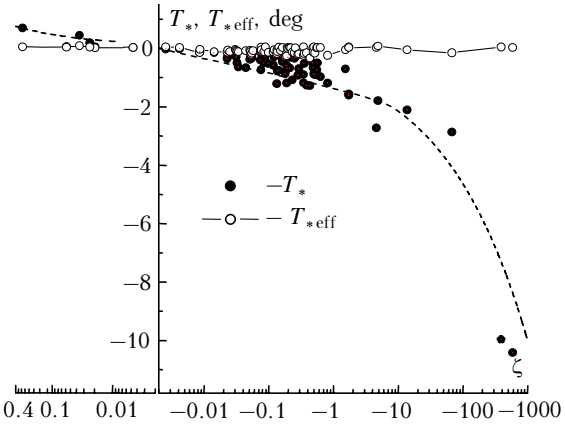

Fig. 23. Comparison of the temperature turbulent scale T_* for the anisotropic boundary layer with the effective scale $T_{*\text{eff}}$ for the isotropic layer: $T_* \sim 4\zeta$ deg, $\zeta > \zeta_*$ ($\zeta_* = -0.125$); $T_* \sim -(-\zeta)^{+1/3}$ deg, $\zeta < \zeta_*$; $\langle T_{*\text{eff}}\rangle = -0.066$ deg.

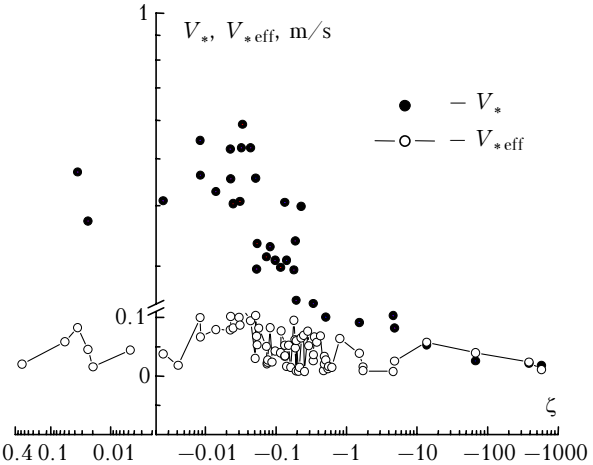

Fig. 24. Comparison of the turbulent scale of velocity V_* (friction velocity) for anisotropic boundary layer with the effective scale $V_{*\text{eff}}$ for the isotropic layer: $V_* \sim 0.27$ m/s, $\zeta > \zeta_*$ ($\zeta_* = -0.125$); $V_* \sim 0.14\ (-\zeta)^{-1/3}$ m/s, $\zeta < \zeta_*$; $\langle V_{*\text{eff}}\rangle = 0.049$ m/s.

Effective scales of an isotropic layer averaged over all observation points turn to be: $\langle T_{*\text{eff}}\rangle = -0.07$ deg, $\langle V_{*\text{eff}}\rangle = 0.05$ m/s. Such values of scales at $z = 2.7$ m and $T_{\text{eff}} = 273.7$ K correspond to the Monin–Obukhov number of an effective isotropic layer: $\langle\zeta_{\text{eff}}\rangle = -0.5$. The specified values of three parameters completely characterize an effective isotropic layer corresponding to actual mountain boundary layer. Parameter $\langle\zeta_{\text{eff}}\rangle$ can serve as the indicator of the general meteosituation above the mountain region under study during the experiments.

Thus, if values of $\langle T_{*\text{eff}}\rangle$, $\langle V_{*\text{eff}}\rangle$, and $\langle\zeta_{\text{eff}}\rangle$ characterizing an effective isotropic layer, are found, then it is possible to use formulas (11) misregarding the anisotropy functions $\varphi_T(\zeta)$ and $\varphi_V(\zeta)$.

4. Outer scale of turbulence in anisotropic boundary layer

As is generally known, the outer scale of turbulence L_0 can be determined variously. For example, V.I. Tatarsky[3] determines the vertical outer scale based on the equality of mean square of difference of random temperature values in two points z_1 and z_2 and its systematic difference.[3] This condition gives

$$C_T^2|z_1 - z_2|^{2/3} = (\mathrm{d}T/\mathrm{d}z)^2\,|z_1 - z_2|^2;$$
$$L_0^{\mathrm{T}} = |z_1 - z_2|/(\alpha C_\theta)^{3/4} = \{C_T^2/[\alpha C_\theta(\mathrm{d}T/\mathrm{d}z)^2]\}^{3/4}, \quad (12)$$

where $\alpha = Pr^{-1} \approx 1.17$; C_θ is the Obukhov constant. The outer scale L_0^{D} can be determined by deviation of structural function of temperature fluctuations from the 2/3-dependence. In space of Fourier-transformations this scale corresponds to L_0^{V} determined from deviations of one-dimensional spatial or temporal frequency spectra from the 5/3-dependence. There are also scales, which are parameters in various theoretical models of the power interval of a three-dimensional fluctuation spectrum (for example, the Karman outer scale L_0^{K}). Practically, it is interesting to find relations between these scales, to obtain their theoretical representations suitable for anisotropic boundary layer, and to compare the results of the theory and experiment.

For the Karman model of a three-dimensional turbulence spectrum the structural function $D(r)$ and one-dimensional spectral density $V(k)$ are set by the expressions[3]

$$D_\nu(r) = 2a_\nu^2\,[1 - 2^{1-\nu}\Gamma^{-1}(\nu)(r/r_0)^\nu K_\nu(r/r_0)];$$
$$V_\nu(k) = \Gamma^{-1}(\nu+1/2)\Gamma^{-1}(\nu)\pi^{-1/2}a_\nu^2 r_0(1+k^2r_0^2)^{-\nu-1/2}, \quad (13)$$

where r_0 is a certain spatial scale (correlation radius); a_ν^2 is the dispersion; K_ν is the McDonald function.

In case of temperature fluctuations, for example, $\nu = 1/3$, $r_0^{-1} = k_0 = 2\pi/L_0^{\mathrm{K}}$, where L_0^{K} is the Karman outer scale.

Expand $D_\nu(r)$ and $V_\nu(k)$ at $\nu = 1/3$ into a series in terms of degrees of r/r_0, k_0/k, and at $\nu = 4/3$ (supposing $r_0 = r_1$, $k_0 = k_1$) – in terms of degrees of r/r_1, k_1/k. Then we obtain

$$D_{1/3}(r) = \alpha_0 r^{2/3} - \alpha_1 r^2 + \mathrm{O}((r/r_0)^{8/3}),$$
$$V_{1/3}(k) = \beta_0 k^{-5/3} - \beta_1 k^{-11/3} + \mathrm{O}((k_0/k)^{17/3}),$$
$$D_{4/3}(r) = \alpha_2 r^2 + \mathrm{O}((r/r_1)^{8/3}),$$
$$V_{4/3}(k) = \beta_2 k^{-11/3} + \mathrm{O}((k_1/k)^{17/3}),$$

where α_0, α_1, β_0, and β_1 are positive constants depending on $a_{1/3}^2$ and r_0; α_2 and β_2 depending on $a_{4/3}^2$ and r_1. Quantities $a_{1/3}^2$, r_0 and $a_{4/3}^2$, r_1 can be related to each other under conditions $\alpha_0 = C_T^2$, $\alpha_2 = (\mathrm{d}T/\mathrm{d}z)^2$, which follow from Eq. (12). They allow one to relate the Tatarsky scale to others.

Determine the outer scale L_0^{V} ($k_* = 2\pi/L_0^{\mathrm{V}}$) from the condition of intersecting $V_{1/3}(k)$ and $V_{4/3}(k)$ in the point k_*, in which relative deviation $V_{1/3}(k)$ from $\beta_0 k^{-5/3}$ (corresponding to the inertial interval) is equal to the set value of δ_{V}. Similarly, determine the outer scale L_0^{D} ($L_0^{\mathrm{D}} = r_* / (\alpha C_\theta)^{3/4}$) from the condition of intersecting $D_{1/3}(r)$ and $D_{4/3}(r)$ in the point r_*, in which relative deviation of $D_{1/3}(r)$ from the inertial interval (dependences $\alpha_0 r^{2/3}$) is equal to the value of δ_{D}. The deviations δ_{V} and δ_{D} turn to be related, for example, at $|\delta_{\mathrm{V}}| << 1$ we have $|\delta_{\mathrm{D}}| \approx 1.14\,|\delta_{\mathrm{V}}|^{3/4}$.

Thus, we have four differently determined outer scales: L_0^{T}, L_0^{K}, L_0^{V}, and L_0^{D}. At small deviations δ_{V}, δ_{D} all these scales are linearly dependent (with awkward expressions for coefficients). For example, at $\delta_{\mathrm{V}} = 0.3$ ($\delta_{\mathrm{D}} \approx 0.37$) the following scale representations through the Tatarsky scale can be obtained:

$$L_0^{\mathrm{V}} \approx 7.3 L_0^{\mathrm{T}},\ L_0^{\mathrm{D}} \approx 0.72 L_0^{\mathrm{T}},\ L_0^{\mathrm{K}} \approx 12.4 L_0^{\mathrm{T}} \qquad (14)$$

(or representations through the Karman outer scale: $L_0^{\mathrm{V}} \approx 0.6 L_0^{\mathrm{K}}$, $L_0^{\mathrm{D}} \approx 0.06 L_0^{\mathrm{K}}$, $L_0^{\mathrm{T}} \approx 0.08 L_0^{\mathrm{K}}$).

As follows from definitions (5), $C_T^2 = C_\theta \varepsilon^{-1/3} N$. Substitute in this formula the expressions (8) and (9) for ε and N in anisotropic layer. The vertical derivative $\mathrm{d}T/\mathrm{d}z$ can be expressed from Eq. (7), where $D^{\mathrm{T}} = -0.49\,\partial T/\partial x + \partial T/\partial z$. Substituting C_T^2 and $\partial T/\partial z$ in Eq. (12), we find the expression for the Tatarsky outer scale, generalized to the case of an arbitrary anisotropic layer:

$$L_0^{\mathrm{T}} = æz[\varphi(\zeta) + \varphi_{\mathrm{T}}(\zeta)]^{3/4}[\varphi(\zeta) + \varphi_{\mathrm{V}}(\zeta) - \zeta]^{-1/4} \times$$
$$\times\, |\varphi(\zeta) + 0.49 z T_*^{-1} \partial T/\partial x|^{-3/2}. \qquad (15)$$

Setting here $\varphi_{\mathrm{T}}(\zeta) = 0$, $\varphi_{\mathrm{V}}(\zeta) = 0$, $\partial T/\partial x = 0$, we obtain the well-known expression for isotropic layer

$$L_0^{\mathrm{T}} = æz\varphi(\zeta)^{-3/4}[\varphi(\zeta) - \zeta]^{-1/4}. \qquad (15a)$$

A more simple expression[3] $L_0^{\mathrm{T}} = æz/\varphi(\zeta)$ can be applied to isotropic layer, which differs insignificantly from Eq. (15a) in limiting cases of strongly unstable and strongly stable stratifications.

Let us compare the theory and the experiment. For this purpose we make use of different methods for obtaining experimental values of vertical outer scale.

As one of such methods, a substitution in Eq. (12) of C_T^2 and $\partial T/\partial z$ measured values (conditionally term this method "by Tatarsky definition") can be used. As is seen in Fig. 19, experimental values of $\partial T/\partial z$ are found from measurements in the low 5-meter layer (the 5th observation session, only 6 points for $\partial T/\partial z$), which are comparatively few in number. Therefore, to make the comparison more full we use other independent methods allowing restoring the experimental values of the outer scale. These methods can be based on measurement results for temporal frequency spectra of temperature fluctuations.

The samples of temperature frequency spectra $W(f)$, obtained in our measurements at various values of ζ are presented in Fig. 25. It is seen that for all spectra the "5/3" inertial intervals of frequencies f, in which $W(f) \sim f^{-5/3}$, and a saturation in the low frequency region are characteristic. The spectra are well described by the Karman model.

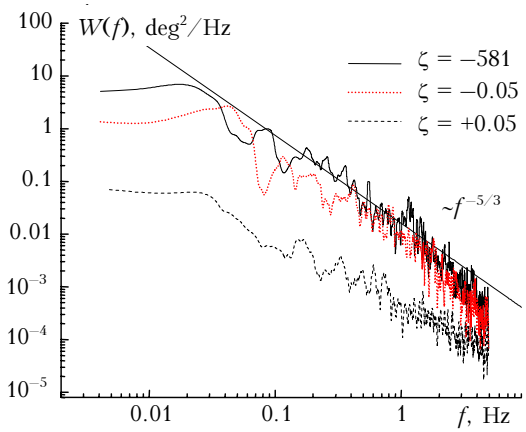

Fig. 25. The experimental non-normalized spectra of temperature fluctuations. The top curve in a low-frequency range corresponds to strongly unstable stratification, bottom one – to stable stratification. Spectra are not smoothed, significant scattering of the points in a high-frequency band results from the discrete Fourier transform.

Apply the Karman spectrum model (13) to definition of the Karman outer scale L_0^{K} by stable characteristics of spectra, for example, by the value of spectra at a lower boundary of the recorded frequency range (denote it as $W(0)$) and the value of the coefficient w_* at the degree $f^{-5/3}$ in the inertial interval ($W(f) = w_* f^{-5/3}$). Make use of the relation[3] $V(k) = vW_{\exp}(kv)$, where v is the modulus of mean wind velocity vector. This relation connects the one-

dimensional spatial spectrum $V(k)$ determined by Eq. (13) with the time frequency spectrum $W_{\exp}(\omega)$, being a standard one-dimensional Fourier transform of the correlation function ($\omega = 2\pi f$). Taking into account that $W(f)$ is a transformation by the positive frequencies and $W(f) = 4\pi W_{\exp}(2\pi f)$, find two methods of definition of the Karman scale L_0^{K} from the spectral characteristics:

$$1)\ L_0^{\mathrm{K}} = 4.8(W(0)v/C_T^2)^{3/5},$$
$$2)\ L_0^{\mathrm{K}} = (v/f)\ \{[W(0)/W(f)]^{6/5} - 1\}^{1/2}. \quad (16)$$

The second method for frequencies of the inertial interval becomes simpler and yields $L_0^{\mathrm{K}} \approx v[W(0)/w_*]^{3/5}$. Conditionally, we term the first of these methods "from spectra by saturation," and the second one "from spectra by 5/3 dependence."

Figure 26 presents a comparison of experimental and theoretical results for the Tatarsky outer scale in a mountain boundary layer. When using the experimental values of the Karman scale obtained from spectra by methods (16), a coefficient of recalculation of the Karman scale into the Tatarsky scale (14) has been applied, which is suitable for any boundary layer.

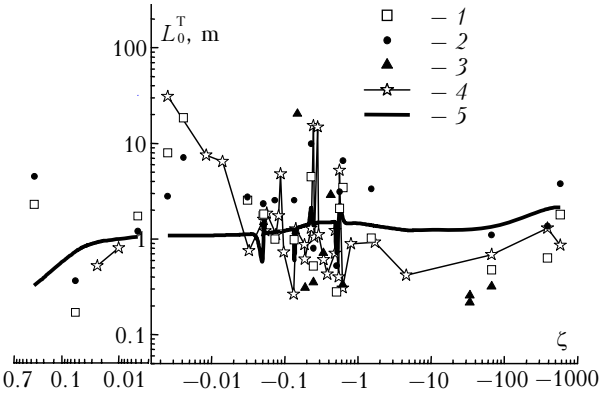

Fig. 26. Comparison of experimental and theoretical results for the outer scale of turbulence L_0^{T} in the mountain boundary layer. (*1*) the experiment (from spectra by 5/3 dependence), (*2*) the experiment (from spectra by saturation), (*3*) the experiment (by Tatarsky definition), (*4*) semiempirical theory for anisotropic layer, (*5*) semiempirical theory for isotropic layer.

Comparison of scales L_0^{T} measured by three different methods ("by Tatarsky definition", "from spectra by saturation," and "from spectra by 5/3 dependence") shows a satisfactory agreement between the experiment and semiempirical theory (15) in an anisotropic boundary layer.

Data of all observation sessions were used (including the 5th altitude observation session) in the comparison. Therefore, because of the evident linear dependence on the height, theoretical scales both of isotropic $L_0^{\mathrm{T}} = æz/\varphi(\zeta)$ and anisotropic layers (15) at some values of ζ (at $z \neq 2.7$ m) jump. As Fig. 26 shows, for such ζ the experimental data also jump. In addition, in the range, where anisotropy is insignificant ($-0.1 > \zeta > -1$) theoretical values of anisotropic and isotropic outer scales, as expected, are close (curves *4* and *5* jump in practically coinciding points of ζ).

In the range of strongly unstable local stratification the anisotropic outer scale is less than isotropic one. As follows from Eq. (15), this decrease is caused by the multiplier $[\varphi(\zeta) + \varphi_V(\zeta) - \zeta]^{-1/4}$, in which the values of $\varphi_V(\zeta) - \zeta$ are high. Both scales (anisotropic and isotropic) decrease in the range of weakly stable stratifications. A noticeable difference between them (anisotropic is larger than isotropic) is observed in the interval of dynamic turbulence (indifferent stratification). The increase of the anisotropic scale is connected with growing $\varphi_T(\zeta)$ in this interval. However, the account for the longitudinal derivative $\partial T/\partial x$ in Eq. (15) bounds the growth of the anisotropic outer scale. As is seen from Fig. 26, it improves the coincidence between the theory and the experiment.

Acknowledgments

The authors thank A.Ya. Bogushevich, V.A. Gladkikh, and S.L. Odintsov for consultations connected with the use of the meteosystem.

References

1. A.S. Monin and A.M. Yaglom, *Statistical Hydromechanics,* Vol. 1 (Nauka, Moscow, 1967), 696 pp.; Vol. 2 (Gidrometeoizdat, St. Petersburg, 1996), 742 pp.
2. A.S. Monin and A.M. Obukhov, Tr. Geofiz. Ins. AN SSSR, No. 24 (151), 163–187 (1954); Dokl. Akad. Nauk **93**, No. 2, 223–226 (1953).
3. V.I. Tatarsky, *Wave Propagation in the Turbulent Atmosphere* (Nauka, Moscow, 1967), 548 pp.
4. L.D. Landau and E.M Lifshitz, *Fluid Mechanics* (Pergamon Press, Oxford, 1969).
5. A.S. Monin, *Hydrodynamics of Atmosphere, Ocean and the Earth Interior* (Gidrometeoizdat, St. Petersburg, 1999), 524 pp.
6. S.S. Zilintinkevich, *Dynamics of the Atmospheric Boundary Layer*, (Gidrometeoizdat, Leningrad, 1970).
7. A.S. Gurvich, Izv. Akad. Nauk SSSR, Fiz. Atmos. Okeana **1**, No. 1 (1965).
8. V.N. Kozhevnikov, *Atmospheric Perturbations at Mountain Flows* (Nauchnyi Mir, Moscow, 1999), 160 pp.